Mantle structure and composition to 800-km depth beneath southern Africa and surrounding oceans from broadband body waves

R.E. Simon[a,b], C. Wright[a,*], M.T.O. Kwadiba[a,c], E.M. Kgaswane[a,1]

[a] *Bernard Price Institute of Geophysical Research, The University of the Witwatersrand, Johannesburg, Private Bag 3, Wits 2050, South Africa*
[b] *Department of Physics, University of Botswana, Private Bag UB704, Gaborone, Botswana*
[c] *Department of Geological Survey, Private Bag 14, Lobatse, Botswana*

Abstract

Average one-dimensional P and S wavespeed models from the surface to depths of 800 km were derived for the southern African region using travel times and waveforms from earthquakes recorded at stations of the Kaapvaal and South African seismic networks. The Herglotz–Wiechert method combined with ray tracing was used to derive a preliminary P wavespeed model, followed by refinements using phase-weighted stacking and synthetic seismograms to yield the final model. Travel times combined with ray tracing were used to derive the S wavespeed model, which was also refined using phase-weighted stacking and synthetic seismograms. The presence of a high wavespeed upper mantle lid in the S model overlying a low wavespeed zone (LWZ) around 210- to ~ 345-km depth that is not observed in the P wavespeed model was inferred.

The 410-km discontinuity shows similar characteristics to that in other continental regions, but occurs slightly deeper at 420 km. Depletion of iron and/or enrichment in aluminium relative to other regions are the preferred explanation, since the P wavespeeds throughout the transition zone are slightly higher than average. The average S wavespeed structure beneath southern Africa within and below the transition zone is similar to that of the IASP91 model. There is no evidence for discontinuity at 520-km depth. The 660-km discontinuity also appears to be slightly deeper than average (668 km), although the estimated thickness of the transition zone is 248 km, similar to the global average of 241 km. The small size of the 660-km discontinuity for P waves, compared with many other regions, suggests that interpretation of the discontinuity as the transformation of spinel to perovskite and magnesiowüstite may require modification. Alternative explanations include the presence of garnetite-rich material or ilmenite-forming phase transformations above the 660-km discontinuity, and the garnet–perovskite transformation as the discontinuity.

Keywords: Body waves; Discontinuities; Kaapvaal craton; Low wavespeed zone; Transition zone

1. Introduction

In the present study, we take advantage of the high density of seismic stations and the high quality and great quantity of the database of the Kaapvaal craton seismological project to define the average body

* Corresponding author. Fax: +27-11-717-6579.
E-mail address: wrighto@geosciences.wits.ac.za (C. Wright).
[1] Present address: Council for Geoscience, Private Bag X112, Pretoria 0001, South Africa.

wavespeed structure beneath southern Africa and surrounding oceans from broadband body waves to depths of about 800 km. This work complements the previous studies (e.g. Qiu et al., 1996; Zhao et al., 1999) by improving the resolution of deep-seated subtle features. It is also an extension of the work of Simon et al. (2002) and Wright et al. (2002). We summarize the P wavespeed results reported by Simon et al. (2002) and present an average S wavespeed model for this region. We compare the P wavespeed results with the preferred model (SATZ) of Zhao et al. (1999) because it was derived using a similar kind of data for a region just to the north of the present study area. The recent Generalised Northern Eurasia Model (GNEM) of Ryberg et al. (1998) for northern Eurasia allows a comparison with the upper mantle and transition zone below a region in a different continent. The S wavespeed results are compared with those of previous shear wave models obtained for southern Africa (Cichowicz and Green, 1992; Qiu et al., 1996; Zhao et al., 1999). A comparison with the IASP91 model of Kennett (1991a) is also provided since it is a fairly recent reference wavespeed model in which the upper mantle component is weighted by data from both oceanic and continental regions.

2. Data acquisition and selection

Data used in this study are from local and regional earthquakes and mining-induced tremors recorded by the Kaapvaal craton broadband seismic network supplemented by data from the South African network at short distances (Simon et al., 2002; Wright et al., 2002). The Kaapvaal craton network consisted of approximately 80 broadband stations that formed part of the international Kaapvaal craton programme (Carlson et al., 1996, 2000). The seismometers were deployed at locations across southern Africa from April 1997 through April 1999, with about 50 stations operating at any one time. The project involved universities in Botswana, South Africa, Zimbabwe, the mining industry in southern Africa and two American research institutions: the Carnegie Institution of Washington and the Massachusetts Institute of Technology. The digital data consist of continuous three-component recordings of seismic waves recorded at 20 samples/s. The broadband seismometers formed a grid network with an average spacing of about 100 km (Fig. 1).

In this work, the mantle structure to depths of 800 km mainly beneath southern Africa, but with some weighting from surrounding oceans at depths below 200 km, is investigated using travel times and waveforms from body waves. We select broadband seismograms from the Kaapvaal craton experiment, concentrating on data from regional and teleseismic earthquakes at epicentral distances of less than 34° (Fig. 1). This experiment recorded many tectonic earthquakes occurring on the African continent and below the surrounding oceans, and yielded waveforms that include relevant arrivals from upper mantle triplications of the travel-time curves that are caused by both the 410- and 660-km discontinuities. Hypocentral data were obtained from the Preliminary Determination of Epicentre bulletins issued by the United States Geological Survey.

3. P wave models

The travel times used by Simon et al. (2002) are in the range 0–34°, which provides information from the surface to depths of about 800 km. These travel times (Fig. 2) comprised 15 tectonic earthquakes and 14 mining-induced tremors that occurred on the periphery of the Witwatersrand basin recorded by the Kaapvaal network, and 120 events recorded by the South African network. A detailed description of the method used to estimate the baseline correction for each event and relative origin time errors was provided by Wright et al. (2002). For events beyond the 15° distance, resolution of the 410- and 660-km discontinuities has been improved by using the phase-weighted stacking technique (Schimmel and Paulssen, 1997) to identify later P wave arrivals of different slownesses associated with triplications in the travel times. For P wave work, all seismograms were filtered between 0.4 and 4.0 Hz. The seismograms were stacked at different slownesses to enhance coherent signals and diminish the amount of random and signal-generated noise.

Because the data used by Simon et al. (2002) differed slightly at short distances from those of Wright et al. (2002), due to the addition of two extra events at distances less than 20°, the P wavespeeds in

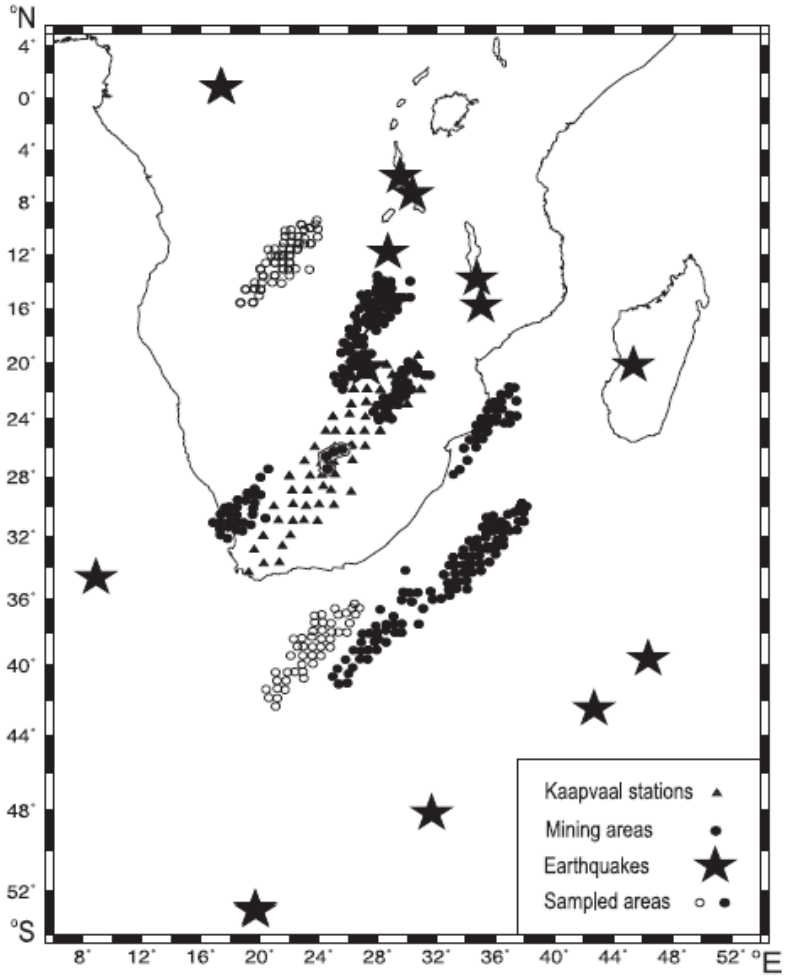

Fig. 1. Map showing locations of mine tremors and earthquakes recorded by broadband stations of the Kaapvaal craton network used in the present study. The four enclosed small stars show the main areas of mining-induced seismicity: from bottom to top—Welkom, Klerksdorp, Far West and West Rand, Central and East Rand. The map shows big stars, triangles, closed circles and open circles denoting earthquake source locations, the Kaapvaal craton broadband station locations, sampled areas above and within the transition zone and sampled areas below the transition zone, respectively. The circles define the midpoints between sources and stations.

the crust and upper mantle show small differences from model BPI1 derived by Wright et al. (2002) which extends to 320-km depth. Therefore, the revised model was denoted BPI1A. The deeper part of the average P wavespeed model was constructed by evaluating the Herglotz–Wiechert integral (Aki and Richards, 1980, pp. 643–651) to provide a preliminary smooth model. The method of constructing the preliminary P wavespeed model and the subsequent refinements were described in Simon et al. (2002). The refinements involve ray tracing, and use of later arrival times obtained from the phase-weighted stack

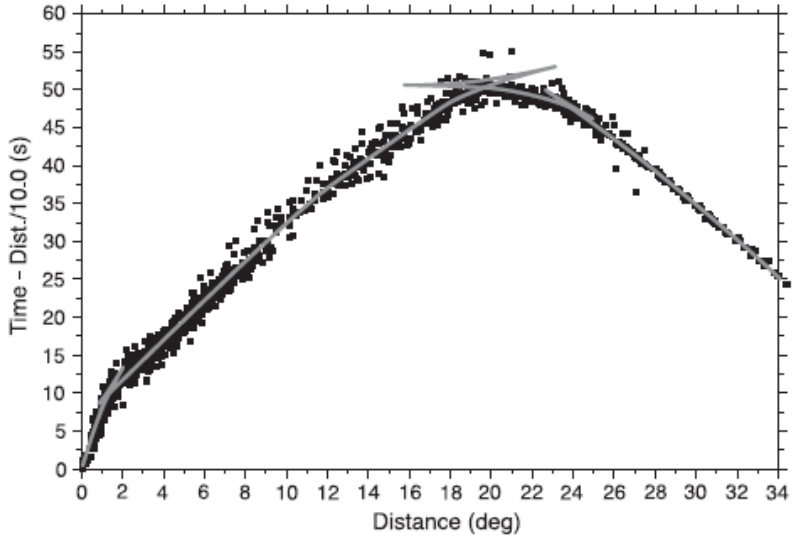

Fig. 2. Plot showing all P wave first-arrival times used in the travel-time analysis from both the Kaapvaal craton and South African networks, with baseline corrections applied, and overlain with the reduced travel-time curve from model BPI1A with $V_{red} = 10.0$ km/s (after Simon et al., 2002).

and synthetic seismograms to define the triplications associated with the major discontinuities. The synthetic seismograms were generated using the WKBJ technique (Chapman, 1978). The resulting travel-time curve is shown in Fig. 2, superimposed on all corrected first arrival times used in the travel-time analysis from both the Kaapvaal and South African networks.

According to Simon et al. (2002), the wavespeeds of BPI1A (Fig. 3) from the base of the crust to 270-km depth lie between those of the SATZ model and the IASP91 model, which have higher and lower wavespeeds, respectively. Between depths of 270 km and the 410-km discontinuity, models BPI1A, IASP91 and SATZ have similar wavespeeds. Model GNEM for Eurasia has lower wavespeeds than the other three models above the 410-km discontinuity. Within the transition zone, models BPI1A and SATZ converge as the depth increases, with wavespeeds exceeding those of IASP91 below 500-km depth. These models and model GNEM all have similar wavespeeds below 750-km depth. Both major discontinuities in BPI1A show similar patterns to those in North America reported recently by Neves et al. (2001) from waveform inversion of broadband seismic data using a genetic algorithm. Model BPI1A shows that the transition zone average thickness is approximately 248 km. The travel times from events with turning points shown as open circles in Fig. 1 reveal that the mantle beneath the transition zone, below both the continental and oceanic regions, has similar properties.

4. S wave models

S wave first arrivals from events with body wave magnitudes between 4.0 and 5.8 have been used to investigate the S wavespeed structure of the mantle beneath the southern African region. The horizontal-component broadband recordings were rotated to radial and transverse components and then band-pass filtered from 0.2 to 2.0 Hz before picking the travel times. Fig. 4 shows all the SV travel times used from the tectonic events. Although the data are generally scattered, most of the stations have reasonably clear S wave arrivals. This scatter appears to be predominant for stations of epicentral distances between 18° and

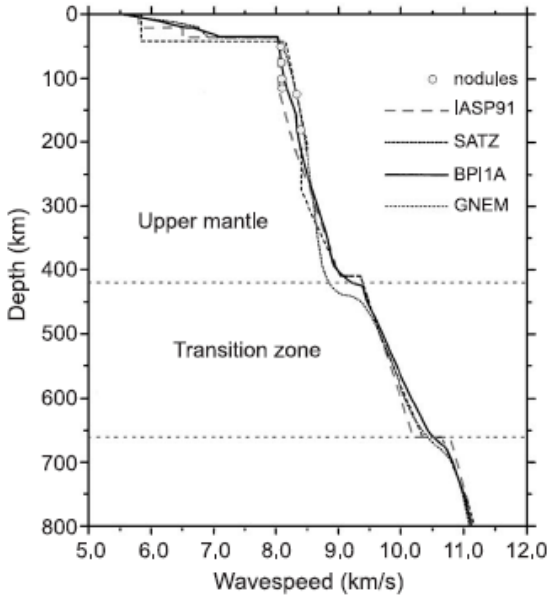

Fig. 3. Comparison of P wavespeed models: IASP91 (Kennett, 1991a), SATZ (Zhao et al., 1999), BPI1A (Simon et al., 2002) and GNEM (Ryberg et al., 1998). The gray circles denote values of P wavespeed for mantle xenoliths estimated by Qiu et al. (1996).

23.5° (Fig. 4), and may be due to complexity in the S wave structure of the mantle above the transition zone below the continental and oceanic lithospheres, or to errors in picking (i.e. phase misidentification) of the S wave arrivals due to the complexity of the P coda resulting from scattering (Kaiho and Kennett, 2000). It appears that at these distances, travel times from continental events are slightly longer than those from oceanic events. SH times show similar variations to those of Fig. 4, and fit a model not significantly different from that derived from SV arrivals. Thus, we are not able to isolate any effect due to anisotropy, and the following discussion is confined to results from SV arrivals.

Because of the large scatter in the S wave data, the Herglotz–Wiechert inversion was not performed, even though the travel times are reasonably uniformly distributed to epicentral distances of 34°. Instead, we used ray tracing to fit a model to the S wave travel times. The starting model was calculated from the P wavespeed model, assuming a constant Poisson's ratio of 0.25. Iterative ray tracing was then used to fit a model to the travel times. The results were then compared with the travel times predicted by the IASP91 shear wave model (Fig. 4). All S wave data were adjusted for origin time errors using corrections computed for the P wave data from the same events used by Simon et al. (2002). The wavespeed model, which gave the best fit to the observed data, was taken as a smoothed approximation to the actual average S wavespeed distribution for this region. The phase-weighted stacking technique (Schimmel and Paulssen, 1997) was then used to identify later shear wave arrivals of different slownesses associated with the upper mantle triplications for both the 410- and 660-km discontinuities, thereby enabling the adjustment of the wavespeeds close to the discontinuities. In addition, synthetic seismograms were generated to assist in using the results from the phase-weighted stacking to refine the model in exactly the same manner as the P wave data. The depths of the 410- and 660-km discontinuities were constrained to lie within 10 km of the corresponding discontinuities for P waves.

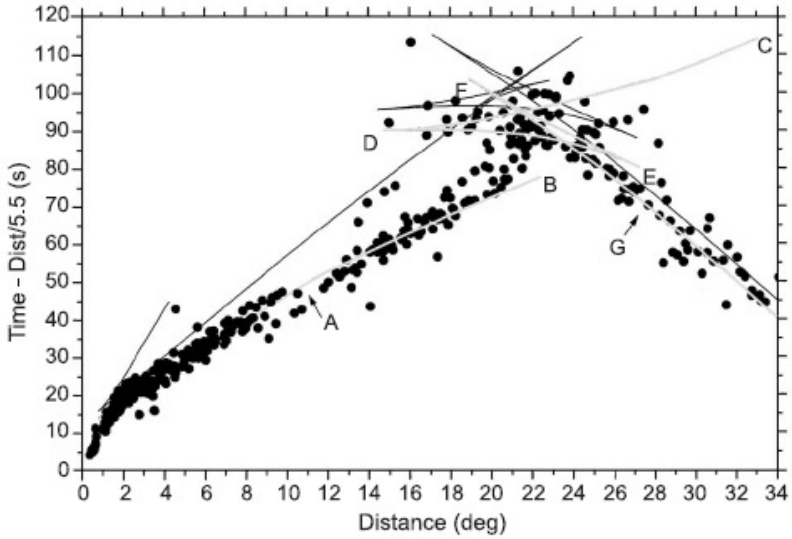

Fig. 4. Plot showing all SV first arrival times used in the travel-time analysis from the Kaapvaal craton network, with baseline corrections applied, and overlain with the reduced travel time curves from shear wave models IASP91 (dark) and BPISM (gray) with V_{red} = 5.5 km/s. For BPISM, travel time branches are as follows: AB—arrivals from the mantle above the LWZ; CD—refracted energy below the LWZ and wide-angle reflections from the top of the 410-km discontinuity; DE—refracted arrivals from within the transition zone; EF—wide angle reflections from the top of the 660-km discontinuity; FG—refracted arrivals from the lower mantle.

The final reduced travel-time curve for S waves is overlain on times measured from tectonic- and mining-induced events recorded by the Kaapvaal network (Fig. 4). Fig. 5 shows seismograms from six earthquakes to illustrate the rapid decrease in first arrival amplitudes of S beyond distances of 19°, which provides evidence for the presence of the low wavespeed zone (LWZ) shown in Fig. 6. The retrograde branches associated with the LWZ and 410-km discontinuity and with the 660-km discontinuity are well defined, and the width of triplication associated with the 660-km discontinuity is much greater than for P waves. The travel-time curve was computed from the average S wave model (BPISM) derived from this work, which is shown in Fig. 6. Other recently published S wave models for this region extend only to depths of 500 km, and include those from Cichowicz and Green (1992), Qiu et al. (1996) and Zhao et al. (1999). Because the models of Zhao et al. (1999), Cichowicz and Green (1992) and Qiu et al. (1996) [hereafter referred to as Vp_Poisson, CGSM92 and QSM96, respectively] are all deficient in some way, we chose not to provide their travel times here. The problems are evident from Fig. 8 of Zhao et al. (1999), which shows that beyond the triplication associated with the 410-km discontinuity, none of the models presented in their work is consistent with their observed data. However, our shear wavespeed model shows travel times that are consistent with observed data up to 34°. Although the observed data show that there is energy arriving where the shadow zone is expected after 22.4° (Fig. 5), this is probably diffracted energy that is not explained by ray theory. The observed shear wave data in Zhao et al. (1999) and our observed data both show a consistent pattern, although in the former, the data are rather sparse beyond distances of 13°.

BPISM provides a better agreement than QSM96 between the seismic wavespeed structure and the wavespeeds estimated by Qiu et al. (1996) from peridotite xenoliths found within the Kaapvaal craton, shown as circles in Fig. 6. This agreement determined from seismology and petrology suggests that the nodules are representative of the average upper mantle

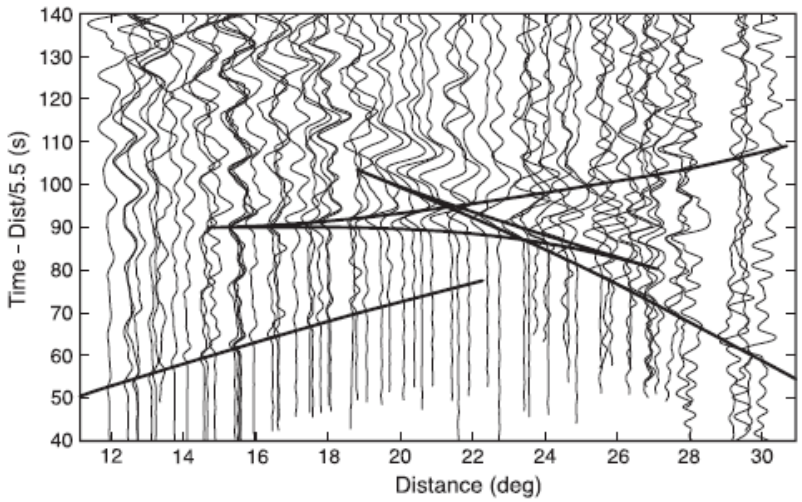

Fig. 5. Composite record section of radial component SV waveforms from tectonic events. The waveforms have been bandpass filtered from 0.2 to 2.0 Hz and overlain with the reduced travel-time curve from model BPISM (V_{red} = 5.5 km/s). The travel-time curves calculated from BPISM and also plotted in Fig. 4 have been superimposed.

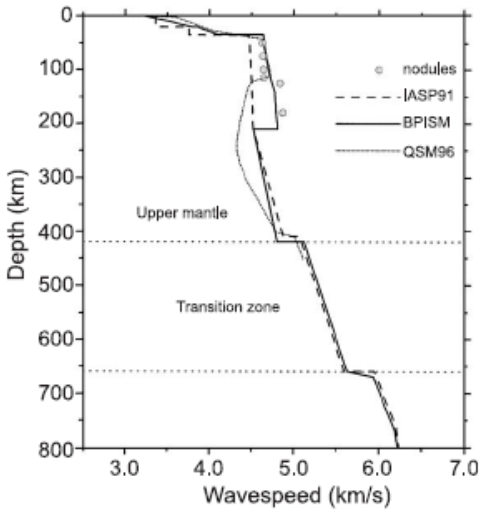

Fig. 6. Comparison of shear wavespeed models IASP91 (Kennett, 1991a), BPISM and QSM96 (Qiu et al., 1996). The gray circles denote values of shear wavespeed for mantle xenoliths estimated by Qiu et al. (1996).

composition beneath this region (Kaapvaal craton with more weighting from the adjacent mobile belts as the depth increases) to depths of 180 km. This is a departure from the QSM96 model, which limits the agreement between seismology and petrology to depths shallower than 120 km. However, our average shear wavespeed model has a LWZ from 210- to ~345-km depths while the LWZ extends from 100 to ~250, 120 to ~400 and 160 to ~350 km in CGSM92, QSM96 and Priestley (1999), respectively. Priestley's (1999) S wave model is a revised version of QSM96 to satisfy both the regional seismic waveform data and the fundamental mode Rayleigh wave data for the region.

The trough in S wavespeed defining the LWZ runs from 4.52 to 4.70 km/s in model BPISM (Fig. 6), while model Vp_Poisson has no LWZ. The LWZ in model BPISM shows a similar pattern to the LWZ in the shear wave model IASP89 (Kennett, 1991b). BPISM generates a shadow zone in the travel-time curve starting at around 22.36° and extends to at least 33.06°, where the reflected energy from below the LWZ starts (points B and C in Fig. 4). Our results

from ray tracing place the base of the LWZ at ~345-km depth, defined by the depth of penetration of refracted energy at point C, which is in close agreement with that of Priestley (1999) that extends to around 350-km depth.

The main features of the data are reasonably well matched by model BPISM (Figs 4, 5 and 6) which is characterized by: a high wavespeed lid, a low wavespeed zone starting at 210 km with a wavespeed drop of ~5.8% and extending to 345-km depth; and two major discontinuities at about 420- and 665-km depth with wavespeed jumps of ~6.7% and ~5.6%, respectively. At the 660-km discontinuity, the data are not capable of unambiguously discriminating between first and higher order discontinuities. The S wavespeed structure below the 410-km discontinuity and throughout the transition zone and below to 800-km depths for the region beneath southern Africa and surrounding oceans generally shows similar characteristics to the P wavespeed distribution (Figs. 3 and 6). The major difference is the evidence for the LWZ around 210-km depth overlain by the high wavespeed upper mantle lid in the S wave model that is absent for P waves.

Above the 210-km depth, the IASP91 S wave model shows wavespeeds that are too slow to be representative of the average wavespeed structure beneath our region of study (Fig. 6). The S wave models BPISM and IASP91 have very minor differences in their wavespeeds within and below the transition zone (Fig. 6). This is evident from the 5 s measured difference (i.e. constant difference over a considerable distance range) in travel-time curves and the similarity in the travel-time slopes of the two models both within and below the transition zone. The systematic difference in travel-time curves is largely due to the upper mantle wavespeed lid in BPISM. This implies that the derived average S wavespeed model of the structure beneath southern Africa within and below the transition zone is similar to that of the global average.

Furthermore, the wavespeeds from model BPISM reveal that the transition zone is approximately 245 km in thickness (248 km from P waves), and these results are consistent with the global average thickness estimates of 241 and 243 km obtained from recent SS precursor studies by Flanagan and Shearer (1998) and Gu et al. (1998), respectively. These estimates are supported by recent results from Gao et al. (2002) who used P-to-S conversions to image the discontinuity structure within the top 1000 km beneath southern Africa from the Kaapvaal seismic data set. They found that the mean mantle transition zone thickness is 245 km. Thus, there is little thinning of the transition zone compared with the global average, and hence temperatures are unlikely to be elevated within the transition zone.

5. Region of applicability of models and errors

Clarification of the properties of the derived P and S wavespeed models can be made with reference to Fig. 1. An unusual aspect of the present models is that they have been constructed from the surface downwards, starting from the region around the Witwatersrand basin, whose northern and western boundaries are defined approximately by the areas of mining-induced seismicity. The top 100 km of the models is broadly representative of the Kaapvaal craton, but become increasingly weighted by information from the surrounding mobile belts as the depth increases. Below depths of about 200 km, information from the oceanic regions and the more northerly regions of the African continent starts to influence the results, until, at the maximum depth of 800 km, the models are weighted averages over a broad region of southern Africa and the oceanic regions to the south. Regional differences in the deep structure are relatively small, detectable, but not accurately resolvable without more data (Simon et al., 2002).

Detailed interpretations of the derived compressional model BPI1A (Fig. 3) and its uncertainties have been described by Simon et al. (2002). The determination of the uncertainties in model BPI1A model has been achieved by using both errors in summary gradients in the fitting of a slowness curve (Bolt, 1978) and cumulative errors in baseline corrections to obtain 95% confidence limits on the wavespeed model through the Herglotz–Wiechert integral (Fig. 7). The intervals just below the Moho depth (Fig. 7), where the dark gray limits spread away from model BPI1A (black line), indicate larger bounds ($\pm$0.12 km/s) compared with the rest of the model that shows average confidence limits of $\pm$0.03 km/s (Simon et al., 2002). The wider bounds below the Moho are due

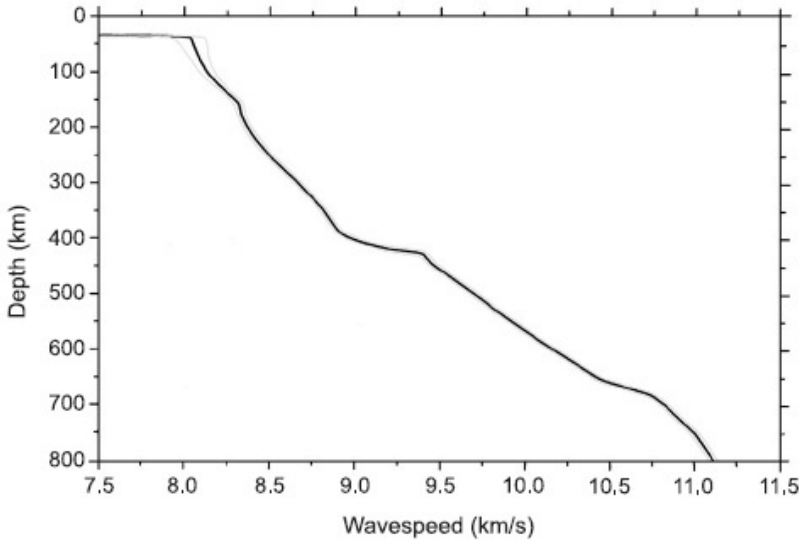

Fig. 7. 95% confidence limits for model BPI1A (dark gray lines) based on the assumption that the assumed sharpness of the 410- and 660-km discontinuities is correct in each case. The error bounds were found assuming fixed crustal wavespeeds to Moho depth (34 km), and have an average deviation of ±0.03 km/s (after Simon et al., 2002).

to the 'hump' observed in the data and from fixing crustal wavespeeds and Moho depth. The error bounds on BPI1A are smaller than those on earlier published models (e.g. Wiggins et al., 1973; Walck, 1984), since they were computed using a probabilistic rather than an extremal method (Simon et al., 2002).

While it is relatively easy to constrain confidence limits on the P wavespeed model, the presence of a LWZ makes this very difficult for S. Because no seismic energy can reach its maximum depth within the LWZ, there is no way of reliably constraining the wavespeeds within the zone from the data alone, and the problem of non-uniqueness in this instance was discussed by Gerver and Markushevitch (1966). The actual wavespeeds within the zone have to be assumed using 'a priori' information, which is the range of petrologically acceptable models. In the present instance, the IASP91 S model (Kennett, 1991a) has been used to constrain the S wavespeeds in the low wavespeed zone.

Reliable statistical estimates of the errors in depths of the 410- and 660-km discontinuities are not easily derived. Perhaps the simplest way of approaching the problem is to stress that a change in depth of either discontinuity of 5 or 10 km for P or S, respectively, results in an observable misfit of the times to those estimated by ray tracing. 5 and 10 km for P and S are therefore approximate values for uncertainties in the depths, subject to the constraint that the errors in the overlying wavespeeds are small.

6. P/S wavespeed ratios

Direct calculations of the P/S wavespeed ratio as a function of depth are particularly valuable, since the main features of the P and S wavespeed distributions were established from the same events (Fig. 8). There are few results for this ratio, which provides insight into temperature variations, partial melting and phase transformations. The reason is that in most parts of the world, P and S models have been constructed by different methods, and using different distributions of events and stations. We estimate the errors in the wavespeed ratio to be about ±0.01 for the upper mantle above the LWZ and the uppermost lower

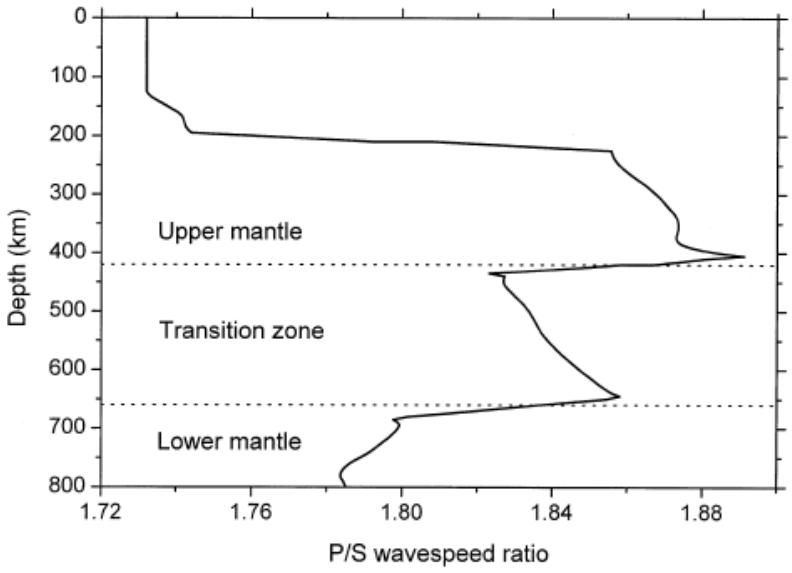

Fig. 8. The wavespeed ratio between P and S waves (P/S) as a function of depth calculated from models BPI1A and BPISM with a moderate amount of smoothing.

mantle, ±0.03 for the LWZ and ±0.02 for the transition zone. From the top of the mantle to depths of 200 km, the wavespeed ratio increases slightly from 1.73 to 1.75, indicating very similar gradients for both P and S waves. This ratio then increases within and below the LWZ from 1.86 at 210 km to 1.92 at 420 km, although the S wavespeeds are poorly constrained from depths of 210 to 420 km. The LWZ is not detected for P waves, and, in such a situation, the LWZ for S is due to temperature gradients alone without partial melting.

At 420-km depth, where the first major discontinuity occurs, the P/S ratio sharply drops from 1.92 to 1.80. However, within the transition zone, the ratio gradually increases from 1.83 to 1.87, indicating a minor reduction in shear wave gradients relative to P. At the base of the transition zone, the ratio sharply drops from 1.87 to 1.79. The sharp drop in ratio upon passing through both boundaries marking the major discontinuities is probably caused by changes in crystal structure, since the increase in wavespeed at these boundaries is due to phase changes inferred from experimental petrology. The P/S ratio stabilizes to values of around 1.79 for the uppermost lower mantle, which is consistent with results from Kennett et al. (1994) who obtained a similar value from their broadband observations for the structure beneath northern Australia. The main features in the P/S wavespeed ratios deduced from our work (Fig. 8) are very similar to those in Kennett et al. (1994) for depths below the 410-km discontinuity through the transition zone down to the lower mantle.

7. The low wavespeed zone in the upper mantle

Our results reflect evidence of a LWZ in S waves in agreement with other studies across southern Africa (e.g. Bloch et al., 1969; Cichowicz and Green, 1992; Qiu et al., 1996; Priestley, 1999; Stankiewicz et al., 2002). However, our model shows greater thickness of the seismic lithosphere (~ 210 km thick) than other studies if the top of the LWZ defines the base of the lithosphere. But these results are inconsistent with those reported by other investigators (Freybourger et al., 2001; James et al., 2001; Gao et al.,

2002) whose results show no evidence of a LWZ for S waves within the Kaapvaal craton. However, we observe from the regions where the rays turn or bottom (Fig. 1) that the LWZ in model BPISM appears to be located outside the craton (i.e. on the cratonic margins and adjacent mobile belts). This probably explains the inconsistency of the results, since sub-cratonic and adjacent continental regions may be different. Our average models reveal that the use of the IASP91 model as a reference model for southern Africa is inadequate in the uppermost mantle, since our models show high wavespeeds compared with the global average. This has important consequences for teleseismic travel-time tomography based on a modified IASP91 model (e.g. results from James et al., 2001). Our results confirm suggestions by Kearey and Vine (1996) that a LWZ is present at a variety of depths between about 80 km and below 300 km, and that it appears to be generally present for S waves beneath stable continental regions, except, possibly, below some Archaean cratons. It may, however, be absent in certain regions for P waves, especially beneath stable continental regions where temperature gradients are lower.

The low seismic wavespeeds could arise from a number of different mechanisms, including an anomalously high temperature, a phase change, a compositional change, the presence of open fluid-filled cracks or fissures and partial melting (Kearey and Vine, 1996). Liebermann and Schreiber (1969) found that critical thermal gradients based upon ultrasonic laboratory data for a great variety of minerals confirm that it is possible to have a LWZ for shear waves without requiring one for compressional waves. Birch (1969) suggested that the LWZ in the upper mantle coincides with a region of increasing iron content. However, Liebermann and Schreiber (1969) argued that there is no compelling evidence that an increase in iron content occurs at depths of less than 400 km. They further point out that in order for the LWZ to be a consequence of partial melting, the LWZ for P and S waves must occur at the same depth. If the S wavespeed decrease is caused by a decrease in the shear modulus, the P wavespeed could decrease at a lesser rate or perhaps not at all, provided that the bulk modulus is increasing fast enough with depth (Dowling and Nuttli, 1964). Anderson and Sammis (1970) suggested that the LWZ should begin and end gradually if it is due to temperature effects. Hence, as a result of these ambiguities, it would be unwise to rule out any of the plausible explanations of the LWZ because they can also occur as a combination.

We interpret the high wavespeeds that persist to depths of ~ 210 km in the shear wave model to indicate that the minimum lithosphere thickness beneath southern Africa is ~ 210 km. However, we note that the LWZ corresponds to the lithosphere beneath the cratonic margins and adjacent mobile belts. Therefore, the cratonic lithosphere could be greater than 210 km thick. This result is consistent with the findings of Ritsema et al. (1998) that the cratonic lithosphere beneath the Tanzania craton is at least 200 km thick. They further argue that the cratonic lithosphere is tectonically "stable" to the extent that it has not been completely destroyed by extensional tectonics that have altered the lithosphere of the younger surrounding mobile belts. A relatively thick (>200 km) cratonic lithosphere is also consistent with the low heat flow from the craton (e.g. Nyblade et al., 1990). Furthermore, our estimate of the lithospheric thickness is comparable to that observed in other regions where ultra-deep diamond inclusions are found, such as the Slave craton in Canada. From their geochemical results, O'Reilly et al. (2001) found that the lithosphere–asthenosphere boundary beneath the Slave craton lies at 200–220-km depth, consistent with the magnetotelluric studies of Jones et al. (2001). The analysis of available Rayleigh wave dispersion data indicates that Precambrian shield areas (such as the Kaapvaal craton) have a deep, relatively rigid, high wavespeed root extending to depths of at least 200 km (Calcagnile, 1991).

The high wavespeeds observed in the upper mantle lid probably indicate a characteristic feature of this region (depleted peridotite), since similar results have been reported from different data sets. These high wavespeeds do not result from neglecting anisotropy because low-frequency surface wave observations (Nataf et al., 1984; Montagner, 1994) show weak anisotropy in the upper mantle beneath southern Africa. The LWZ is of major importance to plate tectonics as it represents a low viscosity layer along which relative movements of the lithosphere and asthenosphere can be accommodated (Kearey and Vine, 1996).

8. Phase transformations

The possible phase transformations in the mantle are shown in Fig. 9. Because the depth of the 410-km discontinuity in model BPI1A closely matches that of the global average, this discontinuity can probably be explained by the transformation of olivine to the β-phase (e.g. Jeanloz and Thompson, 1983). However, the depth and form of the discontinuity are influenced by the pyroxene–garnet transformation, because the two transformations interact through iron partitioning (Weidner and Wang, 2000). The phases that are stable at any depth are influenced by temperature and by variations in aluminium and iron content. As the temperature increases in a mantle of pyrolite composition, the depth of the discontinuity increases, while increases in aluminium and decreases in iron content have the same effect. The preferred depth of the discontinuity (defined by the point of inflection in the wavespeed–depth profile) is 420 km, with an even greater depth suggested by Zhao et al. (1999) for a region of southern Africa to the north of the present study. The slightly greater depth of the discontinuity compared with other regions suggests higher aluminium content and/or iron depletion as the major contributors, since the P wavespeeds are also marginally higher throughout the transition zone (Simon et al., 2002).

Around depths of 550 km, the β-phase transforms to the spinel structure and this transformation is accompanied by a slight increase in seismic wavespeed gradients in some regions, but is not resolved in the present data (Fig. 9). The most distinctive feature of the 660-km discontinuity compared with other regions is the relatively small size of the jump in wavespeed for P, defined by the small lateral extent of the triplication for P, in which the differences in slowness between the two refracted branches are also small compared with the triplication produced by the 410-km discontinuity (Fig. 2). A similar small jump in the P wavespeed at the discontinuity is also present in the results of Zhao et al. (1999) for southern Africa. However, the triplication produced by the 660-km discontinuity appears more pronounced for S (Figs. 4 and 5). Whether this is an effect produced by the 660-km discontinuity itself or is due to differences in frequency content between the high-frequency P arrivals and low-frequency S arrivals remains unclear.

Below the 660-km discontinuity, the dominant phase is perovskite. There are several possible phase

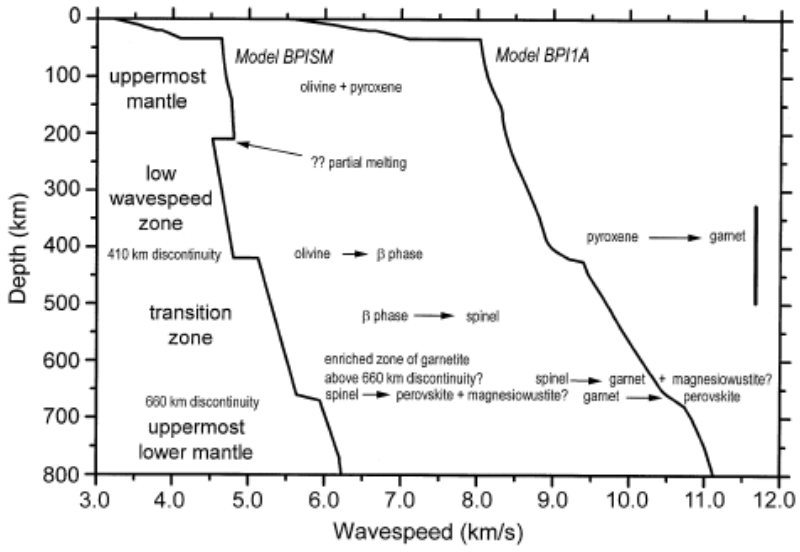

Fig. 9. Possible phase transformations occurring in the mantle superimposed on models BPISM and BPI1A for southern Africa.

transformations which can lead to this (Weidner and Wang, 2000). Garnet may transform partially to ilmenite and then to perovskite, while the spinel (γ) phase may also transform completely to garnet and magnesiowüstite, followed by the garnet to perovskite transformation. Ringwood (1991) interpreted the 660-km discontinuity as a transformation from spinel to perovskite and magnesiowüstite. However, Irifune et al. (1998) reported new data on the breakdown of spinel to perovskite in synthetic forsterite, from which Weidner and Wang (2000) inferred that the spinel form of olivine breaks down first to garnet and magnesiowüstite in a pyrolite transition zone. The garnet would then transform to perovskite at a greater pressure to form the 660-km discontinuity. The magnitude of the 660-km discontinuity is also influenced by the aluminium content (Weidner and Wang, 2000).

Ringwood (1994) discussed the possible accumulation of subducted former oceanic crust to form a gravitationally stable layer of garnetite some 50 km thick on top of the 660-km discontinuity: a process that may have been most effective during the Archaean when mantle temperatures were higher. This would result in an increase in P and S wavespeed gradients towards the base of the transition zone with a consequent reduction of the wavespeed jump at the 660-km discontinuity. The present P and S wavespeed models provide some support for such a process having occurred beneath southern Africa. However, Weidner and Wang (2000) have emphasized that ilmenite-forming transformations could be mistaken for a subducted slab resting on top of the 660-km discontinuity.

9. Conclusions

Observations from broadband body waves confirm the presence of resolvable differences between P and S wavespeed variations above the transition zone. We find evidence of a high wavespeed upper mantle lid in the S wavespeed model overlying a LWZ around 210- to ~345-km depth that is not resolved in the P wavespeed model. The LWZ is representative of the structure beneath the mobile belts adjacent to the Kaapvaal craton, and is most probably a temperature effect. Recent results reported by Stankiewicz et al. (2002) from P-to-S converted waves suggest that a reduced wavespeed gradient zone does exist beneath the Kaapvaal craton, although its depth has remained enigmatic. We estimate the minimum thickness of the lithosphere beneath the periphery of the Kaapvaal craton to be ~210 km. Hence, the lithosphere could be thicker than 210 km beneath the craton, which is consistent with other Precambrian areas. The base of the LWZ beneath southern Africa, which occurs at ~345 km from our S wave model, is consistent with that at ~350 km from Priestley's (1999) results that satisfy both the regional seismic waveform data and the fundamental mode Rayleigh wave data for southern Africa. In the upper mantle, both P and S wave models are in good agreement with wavespeeds estimated from peridotite xenoliths found within the Kaapvaal craton. The sampled area at lithospheric depths (Fig. 1) is dominated by the continental mantle, so that the upper parts of the models are largely representative of the continental lithosphere and similar to models derived for other continental regions.

The 410-km discontinuity shows similar characteristics to that in other continental regions, but appears to be depressed slightly to depths of 420 km. Depletion of iron and/or enrichment in aluminium relative to other regions rather than anomalously high temperatures are the preferred explanation, since the P wavespeeds throughout the transition zone appear to be slightly higher than average. The average shear wavespeed structure beneath southern Africa within and below the transition zone is similar to that of the IASP91 model. There is no evidence for a discontinuity at 520-km depth.

The 660-km discontinuity also appears to be slightly deeper than average (668 km), although the estimated thickness of the transition zone is 248 km for P, which is only marginally greater than the global average of 241 km (Flanagan and Shearer, 1998) or 243 km (Gu et al., 1998). The most interesting feature of the results is the small size of the 660-km discontinuity for P waves compared with many other regions, which suggests that the interpretation of the discontinuity as the transformation of spinel to perovskite and magnesiowüstite may require modification. Possibilities are the presence of a garnetite layer sitting on top of the 660-km discontinuity, ilmenite-forming phase transformations and explanation of the discontinuity as the garnet–perovskite transformation.

Acknowledgements

This research was supported by funding from the National Research Foundation (South Africa), the National Science Foundation (USA), the University Research Council of the University of the Witwatersrand and by mining companies operating in southern Africa. The University of Botswana sponsored R.E. Simon. M.T.O. Kwadiba received financial support from the Government of Botswana and from the Kellogg Foundation (USA), and E.M. Kgaswane from the National Research Foundation and the Council for Geoscience. We thank those who made the Kaapvaal project successful. We thank Alan Jones (Geological Survey of Canada) and two anonymous reviewers for their helpful suggestions towards improving this manuscript.

References

Aki, K., Richards, P.G., 1980. Quantitative Seismology: Theory and Methods, vol. 2. Freeman, San Francisco, pp. 559–932.

Anderson, D.L., Sammis, C., 1970. Partial melting in the upper mantle. Phys. Earth Planet. Inter. 3, 41–50.

Birch, F., 1969. Density and composition of the upper mantle: first approximation as an olivine layer. In: Hart, P.J. (Ed.), The Earth's Crust and Upper Mantle. AGU Monograph, vol. 13, pp. 18–36.

Bloch, S., Hales, A.L., Landisman, M., 1969. Velocities in the crust and upper mantle of southern Africa from multi-mode surface wave dispersion. Bull. Seismol. Soc. Am. 59, 1599–1629.

Bolt, B.A., 1978. Summary value smoothing of physical time series with unequal intervals. J. Comput. Phys. 29, 357–369.

Calcagnile, G., 1991. Deep structure of Fennoscandia from fundamental and higher mode dispersion of Rayleigh waves. Tectonophysics 195, 139–149.

Carlson, R.W., Grove, T.L., de Wit, M.J., Gurney, J.J., 1996. Program to study crust and mantle of the Archean craton in southern Africa. EOS, Transactions, American Geophys. Union 77, 273 and 277.

Carlson, R.W., Boyd, F.R., Shirey, S.B., Janney, P.E., Grove, T.L., Bowring, S.A., Schmitz, M.D., Dann, J.C., Bell, D.R., Gurney, J.J., Richardson, S.H., Tredoux, M., Menzies, A.H., Pearson, D.G., Hart, R.J., Wilson, A.H., Moser, D., 2000. Continental growth, preservation and modification in southern Africa. GSA Today 10, 1–7.

Chapman, C.H., 1978. A new method for computing synthetic seismograms. Geophys. J. R. Astron. Soc. 54, 481–518.

Cichowicz, A., Green, R.W.E., 1992. Tomographic study of upper mantle structure of the South African continent, using waveform inversion. Phys. Earth Planet. Inter. 72, 276–285.

Dowling, J., Nuttli, O., 1964. Travel-time curves for a low velocity channel in the upper mantle. Bull. Seismol. Soc. Am. 54, 1981–1996.

Flanagan, M.P., Shearer, P.M., 1998. Global mapping of topography on transition zone velocity discontinuities by stacking SS precursors. J. Geophys. Res. 103, 2673–2692.

Freybourger, M., Gaherty, J.B., Jordan, T.H., Kaapvaal Seismic Group, 2001. Structure of the Kaapvaal craton from surface waves. Geophys. Res. Lett. 28, 2489–2492.

Gao, S.S., Silver, P.G., Liu, K.H., Kaapvaal Seismic Group, 2002. Mantle discontinuities beneath southern Africa. Unpublished manuscript.

Gerver, M., Markushevitch, V., 1966. Determination of a seismic wave velocity from the travel time curve. Geophys. J. R. Astron. Soc. 11, 165–173.

Gu, Y., Dziewonski, A.M., Agee, C.B., 1998. Global de-correlation of the topography of transition zone discontinuities. Earth Planet. Sci. Lett. 157, 57–67.

Irifune, T., Nishiyama, N., Kuroda, K., Inoue, T., Isshiki, M., Utsumi, W., Funakoshi, K., Urakawa, S., Uchida, T., Katsura, T., Ohtaka, O., 1998. The postspinel phase boundary in Mg_2SiO_4 determined by in situ x-ray diffraction. Science 279, 1698–1700.

James, D.E., Fouch, M.J., VanDecar, J.C., van der Lee, S., Kaapvaal Seismic Group, 2001. Tectospheric structure beneath southern Africa. Geophys. Res. Lett. 28, 2485–2488.

Jeanloz, R., Thompson, A.B., 1983. Phase transitions and mantle discontinuities. Rev. Geophys. 21, 51–74.

Jones, A.G., Ferguson, I.J., Chave, A.D., Evans, R.L., McNeice, G.W., 2001. The electric lithosphere in the Canadian shield. J. Geophys. Res. 103, 15269–15286.

Kaiho, Y., Kennett, B.L.N., 2000. Three-dimensional seismic structure beneath the Australasian region from refracted wave observation. Geophys. J. Int. 142, 651–668.

Kearey, P., Vine, F.J., 1996. Global Tectonics, 2nd ed. Blackwell, Oxford. 333 pp.

Kennett, B.L.N. (Ed.), 1991a. IASPEI 1991 Seismological Tables. Research School of Earth Sciences. Australian National University, Canberra, Australia. 167 pp.

Kennett, B.L.N., 1991b. Seismic velocity gradients in the upper mantle. Geophys. Res. Lett. 18, 1115–1118.

Kennett, B.L.N., Gudmundsson, O., Tong, C., 1994. The upper mantle S and P velocity structure beneath northern Australia from broadband observations. Phys. Earth Planet. Inter. 86, 85–98.

Liebermann, R.C., Schreiber, E., 1969. Critical thermal gradients in the mantle. Earth Planet. Sci. Lett. 7, 77–81.

Montagner, J.P., 1994. Can seismology tell us anything about convection in the mantle? Rev. Geophys. 32, 115–137.

Nataf, H.C., Nakanishi, I., Anderson, D.L., 1984. Anisotropy and shear-velocity heterogeneties in the upper mantle. Geophys. Res. Lett. 11, 109–112.

Neves, F.A., Singh, S.C., Priestley, K., 2001. Velocity structure of the upper mantle discontinuities beneath North America from waveform inversion of broadband seismic data using a genetic algorithm. J. Geophys. Res. 106, 21883–21895.

Nyblade, A.A., Pollack, H.N., Jones, D.L., Podmore, F., Mushayandebvu, M., 1990. Terrestrial heat flow in east and southern Africa. J. Geophys. Res. 95, 17371–17384.

O'Reilly, S.Y., Griffin, W.L., Djomani, Y.P., Natapov, L.M., Pearson, N.J., Davies, R.M., Doyle, B.J., Kivi, K., 2001. The mantle beneath the Slave craton (Canada): composition and architecture. Extended Abstract. The Slave–Kaapvaal Workshop, September 5–9, 2001, Merrickville, Ontario, Canada. Geological Survey of Canada, Ottawa. 5 pp.

Priestley, K., 1999. Velocity structure of the continental upper mantle: evidence from southern Africa. Lithos 48, 45–56.

Qiu, X., Priestley, K., McKenzie, D., 1996. Average lithospheric structure of southern Africa. Geophys. J. Int. 127, 563–587.

Ringwood, A.E., 1991. Phase transformations and their bearing on the constitution and dynamics of the mantle. Geochem. Cosmochim. Acta 55, 2083–2110.

Ringwood, A.E., 1994. Role of the transition zone and 660 km discontinuity in mantle dynamics. Phys. Earth Planet. Inter. 86, 5–24.

Ritsema, J., Nyblade, A.A., Owens, T.J., Langston, C.A., VanDecar, J.C., 1998. Upper mantle seismic velocity structure beneath Tanzania, east Africa: implications for the stability of cratonic lithosphere. J. Geophys. Res. 103, 21201–21213.

Ryberg, T., Wenzel, F., Egorkin, A.V., Solodilov, L., 1998. Properties of the mantle transition zone in northern Eurasia. J. Geophys. Res. 103, 811–822.

Schimmel, M., Paulssen, H., 1997. Noise reduction and detection of weak, coherent signals through phase-weighted stacks. Geophys. J. Int. 130, 497–505.

Simon, R.E., Wright, C., Kgaswane, E.M., Kwadiba, M.T.O., 2002. The P wavespeed structure below and around the Kaapvaal craton to depths of 800 km, from traveltimes and waveforms of local and regional earthquakes and mining-induced tremors. Geophys. J. Int. 151, 132–145.

Stankiewicz, J., Chevrot, S., van der Hilst, R.D., de Wit, M.J., 2002. Crustal thickness, discontinuity depth, and upper mantle structure beneath southern Africa: constraints from body wave conversions. Phys. Earth Planet. Inter. 130, 235–251.

Walck, M.C., 1984. The P wave upper mantle structure beneath an active spreading center: the Gulf of California. Geophys. J. R. Astron. Soc. 76, 697–723.

Weidner, D.J., Wang, Y., 2000. Phase transformations: implications for mantle structure. In: Karato, S., Forte, A.M., Liebermann, R.C., Masters, G., Stixrude, L. (Eds.), Earth's Deep Interior. Mineral Physics and Tomography from the Atomic to the Global Scale. Geophysical Monograph, vol. 117. American Geophysical Union, Washington, DC, pp. 215–235.

Wiggins, R.A., McMechan, G.A., Toksöz, M.N., 1973. Range of earth structure nonuniqueness implied by body wave observations. Rev. Geophys. Space Phys. 11, 87–113.

Wright, C., Kwadiba, M.T.O., Kgaswane, E.M., Simon, R.E., 2002. The structure of the crust and upper mantle to depths of 320 km beneath the Kaapvaal craton, from P wave arrivals generated by regional earthquakes and mining-induced tremors. J. Afr. Earth Sci. 35, 477–488.

Zhao, M., Langston, C.A., Nyblade, A.A., 1999. Upper mantle velocity structure beneath southern Africa from modeling regional seismic data. J. Geophys. Res. 104, 4783–4794.